On the Use of Helicity in Tornado Forecasting

Robert Davies-Jones

[a] *Remote corner of a black hole*

D-J Research Papers, **5**.

31 July 2025

Corresponding author: Robert Davies-Jones, bobdj1066@yahoo.com

ABSTRACT

Hodographs in proximity to violent tornadoes and idealized ones with different shapes and shear distributions are assessed for tornado threat, which is measured by a dynamical significant tornado parameter (DSTP), namely, storm-relative helicity (SRH) from 0 to 1 km times 0-6 km bulk wind difference (BWD) divided by 2000. SRH is computed across layers of different depths to assess the importance of different layers to updraft rotation. The idealized hodographs are purely straight, straight with a right-angle bend at 1 km, and semicircular. Storm motion for a right-moving supercell is customarily estimated as a steering current (the mean 0-6 km wind) plus a fixed propagation (7.5 m s^{-1} to the right of the 0-6 km shear vector).

The bulk shear vector between 0 and 6 km is kept nearly constant and large to support supercells. Introducing the storm-motion formula into the SRH expression decomposes SRH into a mean-wind helicity (MWH) and a propagation helicity (PH). Confining the SRH to the 0-1 km layer makes PH virtually unrepresented in the DSTP for semicircular, bent, and proximity hodographs alike. A storm need not propagate away from the mean wind for the updraft to ingest air with abundant helicity from the lowest kilometer of inflow. Semicircular-shaped hodographs have the greatest tornado potential; unbent straight hodographs the least. The threat increases with concentration of shear near the ground. In the most dangerous environments, PH is smaller than MWH at all heights so updrafts would rotate even if they didn't propagate.

SIGNIFICANCE STATEMENT

Identification of environmental wind profiles that favour tornadoes is an important forecasting issue. The significant tornado parameter, which depends on anticipated storm motion, is a skilful tornado predictor used routinely. I use it to assess the tornado potential of observed and idealized hodographs. Given hodographs with same wind difference between 0 and 6 km but different shapes, I find that the tornado threat is minor for purely straight hodographs, moderate for ones with a low-elevation bend, and high for semi-circular ones. For all these hodographs, threat increases when the wind shear is largest near the ground. I show that in particularly dangerous environments the rotation predictor is little affected by rightward storm propagation relative to the mean wind.

1. Introduction

In forecasting applications, storm motion is unknown in advance. In supercell theory, rotation and propagation are linked. As stated by Weisman and Rotunno (2000, p. 1453), "dynamically induced vertical pressure gradients ... force an updraft to propagate continuously toward a particular flank, thus allowing it to become well correlated with the vertical vorticity on that flank." Davies-Jones (2004) quantified this link. Propagation in the above context means propagation off the hodograph, i.e., relative to the environmental wind at each level. Alternatively, one can define a height-independent propagation velocity by decomposing storm motion into a mean-wind translation velocity and a propagation velocity, usually to the right of the mean wind in the northern hemisphere. This decomposition is the basis of the Bunkers et al. (2000) method for predicting supercell motion.

For idealized hodographs, a tornado predictor is needed to assess their tornado potentials. The significant tornado parameter (STP; Thompson et al. 2003) is a skillful predictor of significant (strong or violent) tornadoes. STP values of 1 discriminates between significantly tornadic and nontornadic supercells and the mean STP for significantly tornadic supercells is 3.4 (Thompson et al. 2003, p. 1258).

The original STP originally was proportional to the storm-relative helicity (SRH) of the 0 to 1 km AGL (above ground level) times the bulk wind difference, (BWD), times some thermodynamic factors. BWD is the magnitude of the bulk shear vector from 0 to 6 km. Since we are considering only the dynamics herein, we define a ‘dynamic STP’ (DSTP), which is obtained by setting the thermodynamic factors to one. DTSP depends only on the hodograph and the actual or predicted storm motion.

The rationale behind the DSTP is as follows. Large BWD is associated with strong thermal winds and jet streams, which are found near fronts and in landfalling hurricanes. Large low-level storm-relative helicity is associated with Ekman veering, warm-air advection, and low-level jets. The environment is thus primed for formation of storms that develop into supercells.

Since the DSTP depends on storm-relative helicity, it can be decomposed into two parts, a mean-wind part and a propagation part. In tornado environments, which part is the dominant one?

The article proceeds as follows. Section 2 describes helicity in greater detail. In section 3, SRH is decomposed into a mean-wind helicity (MWH) and a propagation helicity (SPH).

Sections 4 and 5 discuss the Bunkers et al. method for predicting storm motion and the DSTP. Hodographs with almost the same large BWD, but with very different shapes are studied in Sections 6-9. The DSTPs based on the predicted storm motion and the actual one are calculated to assess the tornado threat in each case. The mean-wind and propagation parts of the DSTP are then computed to assess their relative magnitudes. Section 6 presents two hodographs in proximity to violent tornadoes. These hodographs are very dissimilar. One is almost straight from 0.7 to 7 km AGL, the other approximates a semicircle in the lowest 5 km. In addition, three shapes of idealized hodograph are considered; purely straight hodographs (section 7), straight hodographs with a 90° bend at 1 km height (section 8), and hodographs that are semi-circular from 0 to 6 km (section 9). The curve parameter of a hodograph is height. For the same overall shape and size of hodograph curve, vastly different helicity profiles and tornado potentials occur for different variations of shear with height (i.e., for different distributions of the height labels along the hodograph curve. To illustrate this dependence, each shape category includes a hodograph with constant shear magnitude and one with shear declining with height. Bar charts are used in section 10 to compare the helicities and DSTPs of the different hodographs. Section 11 summarizes the results.

2. Helicity

Davies-Jones (1984) identified storm-relative streamwise vorticity as the origin of updraft rotation in helical storms and Lilly (1986) introduced the important quantity, helicity, into supercell dynamics. In fluid dynamics (and other fields), helicity is important in its own right. For example, it affects turbulent cascade of energy and vortex-line reconnection, and satisfies a conservation law (Lilly 1986). Davies-Jones et al. (1990; hereafter DJBF90) defined storm-relative helicity (SRH) as the integral from zero to three kilometers AGL, or more generally from heights b to h, of the scalar product of environmental vorticity and storm-relative (SR) wind. [Layers are specified by (b:h) notation hereafter where b and h are in km.] The environmental vorticity has the same magnitude as the environmental shear and is directed 90° to the left of it, and the streamwise vorticity is its component in the direction of the SR wind. The SR helicity is minus twice the signed area swept out by the SR wind vector. [A signed area is positive when swept out counterclockwise]. For a fixed layer, the contours of SRH as a function of storm motion on a hodograph diagram are evenly spaced

straight lines (e.g., Fig. 1). In situations with diversely moving storms, a meteorologist can use these contours to identify the storms with the most tornado potential (DJBF90).

The integrand in SRH is the SR helicity density, which is equal to streamwise vorticity times the SR windspeed in the relevant reference frame. It follows from the formula for streamwise vorticity in Davies-Jones (1984) that SR helicity density = (SR windspeed)^2 times the rate at which the SR wind turns clockwise with height. Alternatively, from elementary vector analysis (Kreyszig 1972), the SR helicity density is twice the area of the triangle formed by the shear and adjacent SR wind vectors with the area being positive (negative) when the SR wind is to the left (right) of the shear vector. The SR helicity density is the same for all SR wind vectors with tails that fall along the same line parallel to the shear vector (Fig. 1). The SRH of a layer does not decompose into a layer-mean SR wind and a layer-mean SR streamwise vorticity.

DJBF90 envisioned SRH(0:3) as a useful nowcast predictor of mesocyclones and by association tornadoes. The observed storm motions of individual storms were used to compute SR wind. Since it is twice an area, a forecaster can envision how adding new information such as updated surface winds or changes in storm motion will affect the parameter. It was also intended to be separate from CAPE and CIN as they can vary significantly over short distances and on short time scales (for example near a dryline or warm front, or ahead of a short-wave trough). Furthermore, there are many sources of wind information without accompanying thermodynamic measurements (e.g., profilers, VAD winds, pibals). It was purposely left to forecasters to combine the dynamical and thermodynamical ingredients into their forecast. Helicity is a predictor of the helical nature of storms, which produces *covariance* between vertical velocity and vertical vorticity (i.e., vertical helicity density). It does not pretend to predict other storm characteristics such as convective mode, maximum vertical velocity, maximum vorticity, updraft radius, and updraft mass flux.

The rationale for using SRH instead of streamwise vorticity as a nowcast parameter is as follows. Modelers use nice smooth initial hodographs as initial conditions so they have no problem with differentiating the initial wind profile and thereby computing environmental vorticity. In the real world, the winds are turbulent and the hodograph curve, like a coastline, is a fractal that cannot be differentiated accurately. Normal vectors such as environmental vorticity and tangent vectors such as wind shear are ill-defined. The computed vorticity thus varies with measurement resolution. Partitioning vorticity into storm-relative streamwise and

crosswise components is even more problematic. In contrast, SRH is well behaved as it is proportional to an area and converges to a limit as resolution increases.

When SRH evolved in its present form (DJBF90), there were few levels of wind measurements below 1 km owing to the characteristics of Doppler radars, profilers, and rawinsondes. Furthermore, model soundings were inaccurate. DJBF90 computed SRH over the 0 to 3 km layer to encompass the storm inflow depth. They realized that this depth would not mask near-ground SRH since SRH(1:3) typically is smaller than and has the same sign as SRH(0:1) (Fig. 2). It was recognized however that, for fixed SRH(0:3), tornado threat increased with greater concentration of SRH density near the ground (Church et al. 1993, p. 634). Subsequently, some authors found that SRH(0:1) (Rasmussen 2003; Thompson et al. 2003; Markowski et al. 2003) is a better tornado predictor than SRH(0:3).

Since the surface-based layers have an *arbitrary* fixed depth and supercellular convection is sometimes elevated, Thompson et al. (2007, 2012) and Peters et al. (2020) advocated evaluating SRH over an effective inflow layer (EIL) where the base *b* and top *h* are determined by *arbitrary* fixed parcel CAPE and CIN thresholds, thereby introducing thermodynamics into SRH. Whether a parcel can be lifted to its level of free convection does not depend just on its CAPE and CIN computed from a sounding prior to or ahead of a storm. The ability of parcels to move vertically should depend on its effective buoyancy (Davies-Jones 2003a) and the dynamical pressure-gradient forces that act upon it. Vortex suction (Lilly 1986) can lift up quite negatively buoyant air. For surface-based supercells, the median value of the EIL in Coffer et al.'s (2019) dataset is 2.23 km.

With the advent of more accurate model-forecast soundings, SRH(0:1) has morphed into a forecast parameter, which requires an estimate of storm motion as this is unknown in advance. The Bunkers et al. (2000) technique assumes that supercell motion consists of an advection by the mean wind in the 0-6 km layer plus a propagation velocity away from this mean wind. Figure 1 shows predicted storm motions on an idealized hodograph that typifies the wind profile in supercell environments. The propagation velocity is 7.5 m s^{-1} in a direction that is 90° to the right or left of the bulk shear vector **S** from 0 to 6 km, depending on whether the storm is a right-moving (RM) or left-moving (LM) supercell. The Bunkers'method assumes constant propagation speed when it should be scale invariant. It is evident from Weisman and Klemp (1984, their figure 8) that the propagation speed increases with |**S**(0:6)|.

The debate over the optimum layer for computing SRH continues. Based on model soundings, predicted storm motion and skill scores, Coffer et al. (2019) concluded that SRH(0:0.5) was an even better tornado predictor than SRH(0:1). Figure 2 is a plot of median values of SRH for different layers for non-tornadic, weakly-tornadic and significantly-tornadic supercells. The data are from Coffer et al. (2019). The chances of tornadoes and more significant ones increase with increasing helicity values of all the layers. The greatest spread in SRH across supercell types is for the 0-1 km layer. Furthermore, the significant-tornado environments have a greater percent of their 0-3 km SRH (81%) in the lowest 1 km. For the weakly tornadic and non-tornadic supercell environments, the percentages are 71% and 53%, respectively. Along with high SRH values, greater concentration of helicity near the ground is an important consideration in tornado forecasting. The spread in SRH across supercell types is almost identical for the EIL and 0-3 km layers. Thus, the EIL seems an unnecessary complication.

According to results from high-resolution convection-allowing forecast models, a recent study (Coffer et al. 2025) found that, compared to their predicted motion, strongly tornadic supercells close to tornadogenesis time tend to move slower and further to the right. They concluded that, when current observed storm motions are used, the SRH computed over deeper layers has more tornado-forecasting skill than near-ground SRH.

The optimum layer is decided by small differences in skill score. Thus, the 'best layer' is sensitive to a number of factors such as whether the soundings are actual ones or model ones, which model is used, whether the storm motion is observed or predicted, and whether the proximity sounding is representative of the 'unperturbed environment'.

Using a skill score to forecast supercell type (Rasmussen 2003; Coffer et al. 2019, 2025) leads to inconsistencies. Since adjacent areas are additive, SRH(0:3) = SRH(0:1) + SRH(1:3). Let ∅SRH(b:h) be the optimal value of SRH(b:h) for discriminating significantly tornadic storms from non-tornadic ones. This is the value of SRH(b:h) that has the highest skill score. One naively expects that ∅SRH(0:3) = ∅SRH(0:1) + ∅SRH(1:3), but examination of table 1 in Coffer et al. (2025) shows this is not the case. Unlike mean values. optimal values don't preserve helicity addition. [Nor do the median values if the distributions are skewed.]. An example will help clarify this point. Let the prefix μ denotes mean value. Suppose hypothetically that μSRH(0:1) = 100 and μSRH(0:3) = 310 for non-tornadic storms and μSRH(0:1) = 200 and μSRH(0:3) = 390 for significantly tornadic storms. Since means

preserve addition, μSRH(0:1) + μSRH(1:3) = μSRH(0:3), which implies μSRH(1:3) = 210 for non-tornadic storms and 190 for significantly tornadic storms. Suppose ∅SRH(0:1) = 150 and ∅SRH(0:3) = 350. If ∅SRH(1:3) ≠ 200, the optimal values are inconsistent with helicity addition and their interpretation is questionable.

It is advisable to look at helicity in different layers, as in this paper, to explore physics that is unrepresented in a one-layer index. For left-moving, anticyclonically rotating updrafts, the SRH paradoxically is positive in the shallow 0-1 km layer. From soundings taken in hurricanes, McCaul (1991) investigated the relationships between several predictors and the severities of hurricane tornado outbreaks. Since cell motions were unavailable, he assumed that the mini-supercells that produced the tornadoes were moving with a pressure-weighted 0-6 km mean wind. He reckoned that the mean-wind helicity (MWH) so obtained probably underestimated the SRH by 20-50%. The average MWH(0:3), MWH(0:6), and MWH(0:12) were 234, 330, and 552, respectively. Surprisingly, the 0-12 km mean-wind helicity correlated the best, by a small margin, with the outbreak severities.

According to Esterheld and Giuliano (2008), another factor that enters into the discrimination between significantly tornadic supercells and non-tornadic supercells is surface vorticity that is almost purely streamwise in the SR frame. Rightward propagation generally results in the surface vorticity being more streamwise (Fig. 1). The surface vorticity of the LM supercell in Fig. 1 is partly streamwise. Since upward tilting of streamwise vorticity produces cyclonic vorticity, this would explain why LM supercells with their anticyclonically rotating updrafts rarely produce tornadoes.

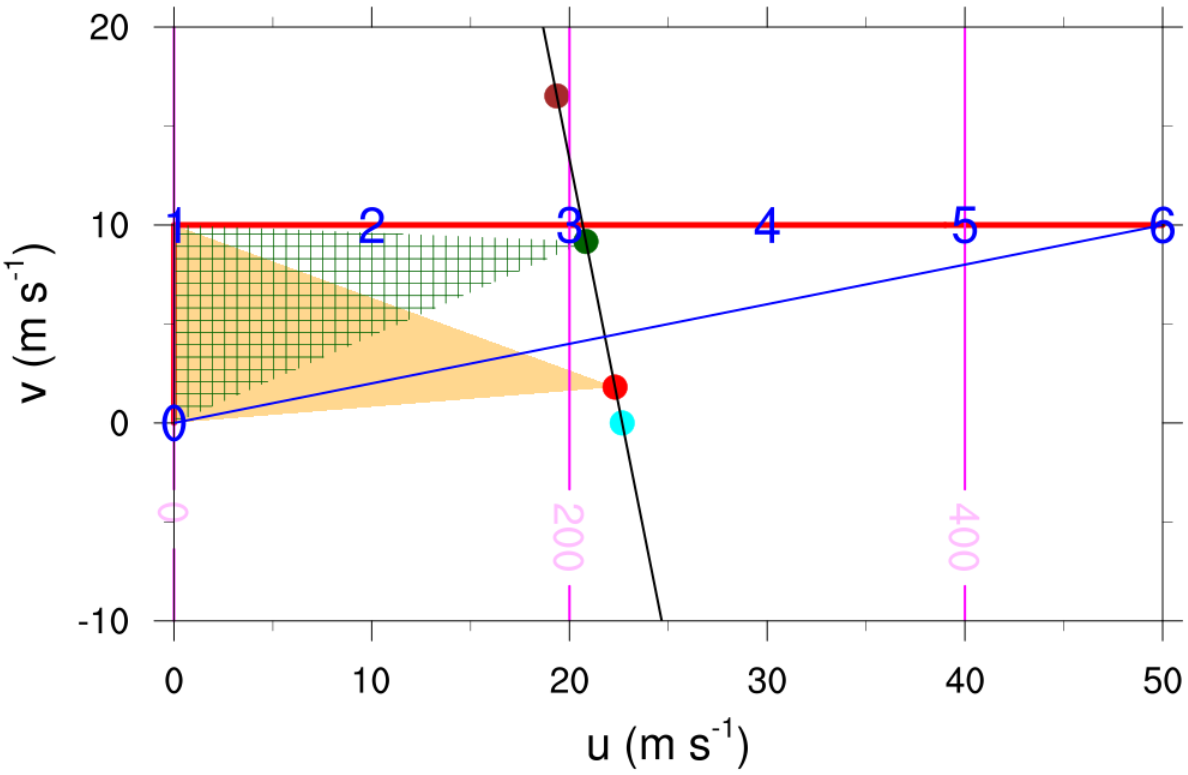

FIG. 1. Illustration of why, in a hodograph with a bend at 1 km AGL, the propagation helicity of the 0 to 1 km layer is small compared to MWH(0:1). This hodograph approximates the wind environment of many tornadic supercells. The hodograph is in red with blue numbers along it denoting heights in km AGL. The green solid dot marks the tip of the mean-wind vector. The black thick line is the line through the mean wind that is perpendicular to **S**(0,6), the 0-6 km bulk shear vector (the blue line). The red and brown dots mark the Bunkers storm motions for the RM and LM supercells, respectively. These are on the black line 7.5 m s^{-1} from the green dot. The areas associated with the 0-1 km MWH and the 0-1 km helicity relative to the RM storm motion are filled in with green hatching and orange, respectively. Areas are positive when swept out counterclockwise by the relevant wind vector as its height varies from 0 to 1 km. Helicities are minus twice the corresponding signed area. The magenta straight lines are 200, and 400 contours of helicity as a function of storm motion. The contour lines of this function are evenly spaced and the zero contour is coincident with the *v*-axis. The 0-1 km SRH is only slightly greater than the 0-1 km MWH so the 0-1 km PH is small. The environmental vorticity vectors have the same magnitude as the shear vectors and are 90 to the left of them. The surface vorticity is westward for this hodograph. The cyan dot marks the storm motion for which the SR surface wind is also westward, thus making the SR vorticity purely streamwise.

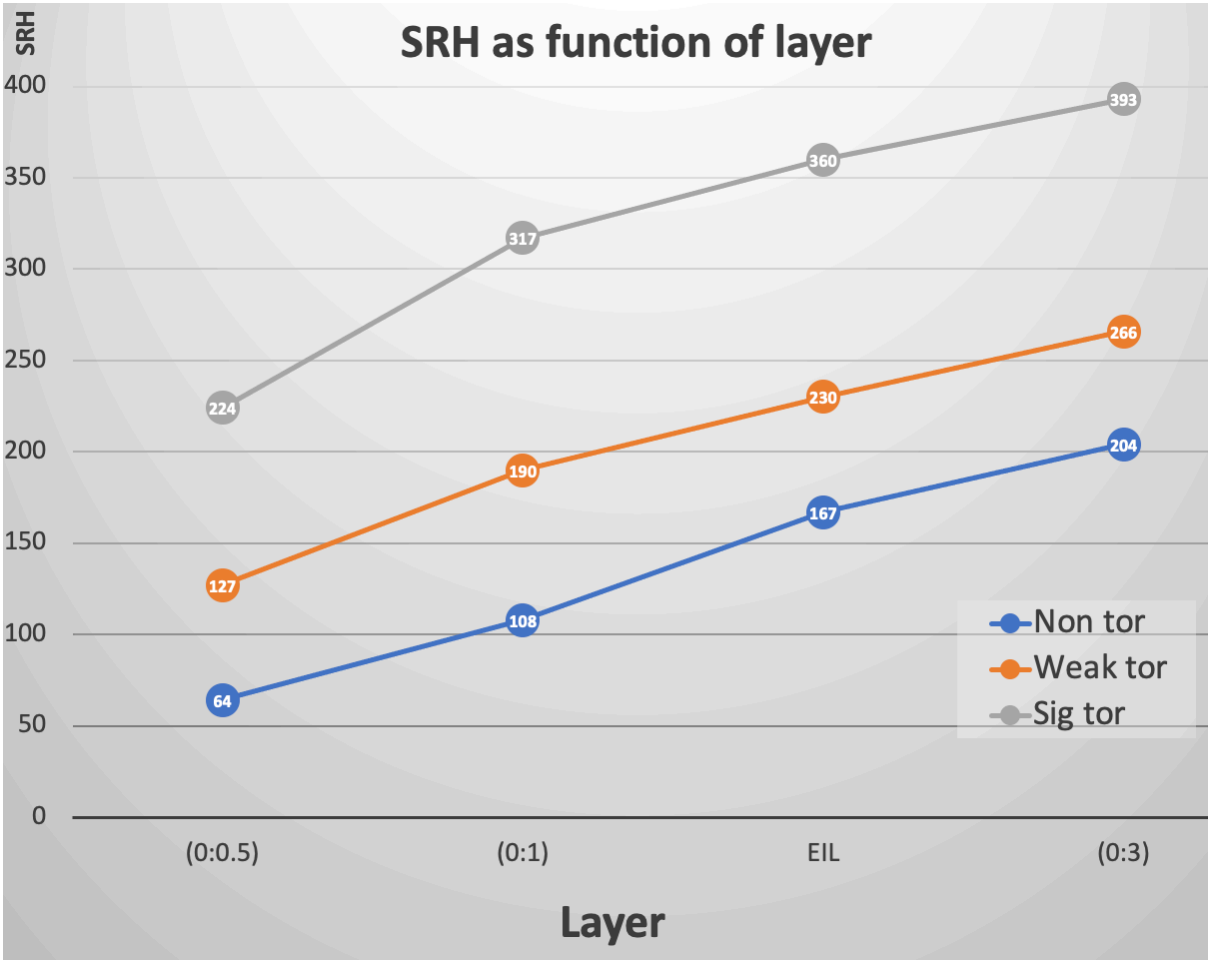

FIG 2. Median values of SRH by different layers for three types of supercells: non-tornadic (blue curve), with weak tornadoes (orange), and with significant tornadoes (grey). The data is from table 2 in Coffer et al. (2019).

3. Mean-wind and propagation helicity

We introduce the following notation. The unit eastward, northward, and upward vectors are **i**, **j**, **k**. The environmental wind at height z AGL is $\mathbf{v}(z) \equiv u\mathbf{i} + v\mathbf{j}$, and the bulk shear vector across a layer is $\mathbf{S}(b{:}h) \equiv \mathbf{v}(h) - \mathbf{v}(b)$ where b and h are the heights of the base and top of the layer. SI units are used implicitly in places. Hence, the units of wind and helicity are m s^{-1} and m^2 s^{-2}, respectively. Although the unit of height is m, specific height values in arguments of functions are given in km for brevity. Thus, $\mathbf{v}(6)$ is the wind vector at 6 km, the 0-1 km SRH is SRH(0:1), etc. The bulk wind difference $\mathrm{BWD} \equiv |\mathbf{S}(0{:}6)| \equiv |\mathbf{v}(6) - \mathbf{v}(0)|$. On a hodograph diagram, z (in km) is the curve parameter and $d\mathbf{v}/dz$ is tangent to the curve. The SRH of a layer is

$$\mathrm{SRH}(b{:}\,h) \equiv \int_{z=b}^{h} [\mathbf{v}(z) - \mathbf{c}] \cdot \mathbf{k} \times \frac{d\mathbf{v}}{dz} dz \tag{1}$$

where **v** is the environmental wind, $d\mathbf{v}/dz$ is the shear vector, $\mathbf{k}\times d\mathbf{v}/dz$ is the environmental vorticity vector (90° to the left of the shear vector), **c** is the storm-motion vector, and SRH(b:h) is twice the area swept out *clockwise* from b to h by the SR wind vector $\mathbf{v}(z) - \mathbf{c}$ (DJBF90). Note that the helicity is positive for an area that is swept out clockwise. Since areas are additive,

$$\mathrm{SRH}(b{:}\,h) = \mathrm{SRH}(b{:}\,\gamma) + \mathrm{SRH}(\gamma{:}\,h) \tag{2}$$

where γ is a third height.

Following Bunkers et al. (2000), we assume that supercell motion consists of a mean-wind steering current $\bar{\mathbf{v}}$ and a propagation velocity **P**,

$$\mathbf{c} = \bar{\mathbf{v}} + \mathbf{P}, \tag{3}$$

where $\bar{\mathbf{v}}$ is the 0-6 km mean wind vector. Then **P** ($\equiv \mathbf{c} - \bar{\mathbf{v}}$) is the deviation of storm motion from the steering current.

By introducing (3) into (1), we obtain

$$\mathrm{SRH}(b{:}\,h) = \mathrm{MWH}(b{:}\,h) + \mathrm{PH}(b{:}\,h) \tag{4}$$

where the mean-wind helicity (Droegemeier et al. 1993) is

$$\mathrm{MWH}(b{:}\,h) \equiv -\int_{b}^{h} \mathbf{k} \cdot [\mathbf{v}(z) - \bar{\mathbf{v}}] \times \frac{d\mathbf{v}}{dz} dz \tag{5}$$

and the propagation helicity is

$$\mathrm{PH}(b{:}\,h) \equiv \int_{b}^{h} \mathbf{k} \cdot \mathbf{P} \times \frac{d\mathbf{v}}{dz} dz\,. \tag{6}$$

The mean-wind helicity is equal to minus twice the signed area swept out by the wind relative to the mean wind. It is the SRH *if* the storm were not propagating. Positive MWH is associated with veering of the vector $\mathbf{v}(z) - \bar{\mathbf{v}}$.

4. Predicted storm motion

Storm motion is not known in advance (except in nowcasting applications) and so has to be predicted. This is done via the Bunkers et al. (2000) method. This procedure assumes that motion of a right-moving supercell consists of two parts, (i) advection of the storm by $\bar{\mathbf{v}}$, the mean wind between 0 and 6 km AGL, and (ii) a fixed propagation velocity **P** away from $\bar{\mathbf{v}}$ at

a 90° angle to the right of **S**(0:6), the shear vector from 0 to 6 km (Fig. 1). [Minor averaging of the head and tail of the shear vector is neglected here for simplicity.] $|\mathbf{P}|$ =7.5 m s^{-1} provides the best fit to the data. Note that the propagation velocity is not scale invariant. It does not vary with the size of the hodograph whereas it should according to theoretical analysis (Davies-Jones 2004). The mean absolute error of the predicted storm motion is not small (4.1 m s^{-1}). The propagation velocity of a left-moving supercell, is similar, but to the left of **S**(0: 6).

Thus, the Bunkers right-moving storm motion is described mathematically by

$$\mathbf{c} = \frac{1}{6}\int_0^6 \mathbf{v}(z)dz + \sigma \mathbf{S}(0\colon 6) \times \mathbf{k} \tag{7}$$

where the first and last terms on the right are the steering current, $\bar{\mathbf{v}}$, and propagation velocity, **P**, and

$$\sigma \equiv 7.5/\mathrm{BWD} = 7.5/|\mathbf{S}(0\colon 6)|\,. \tag{8}$$

Inserting the last term in (7) into (6) and using (8) and vector identities produces

$$\mathrm{PH}(b\colon h) \equiv \sigma \mathbf{S}(0\colon 6) \cdot \mathbf{S}(b\colon h) = 7.5\hat{\mathbf{S}}(0\colon 6) \cdot \mathbf{S}(b\colon h). \tag{9}$$

for the predicted propagation helicity. Here the circumflex denotes unit vector.

The Bunkers method is Galilean invariant, but fails to satisfy a similarity law. Consider for example two parameterized hodograph curves A and B that are identical except A is larger in size by a factor Δ. By similarity, all the bulk wind differences in A, such as the BWD and the mean wind minus the surface wind, should be Δ times larger than in B. In the Bunkers paradigm, however, the propagation speed of the supercell from the mean wind is fixed at 7.5 m s^{-1} for all hodographs, in violation of scale invariance. Compared to B, the propagation in A should be Δ times larger and the SRH (since it is proportional to area on a hodograph diagram) should be Δ^2 times larger. The propagation speed could be made scale invariant by redefining σ as a constant with an optimum value about 0.2.

5. Dynamic STP

The significant tornado parameter is a skillful composite index used in tornado forecasting (Thompson et al. 2003). It is a kludge of other parameters. Ideally, a single

parameter could be used to forecast whether supercells will produce tornadoes. The following illustrates the problem of looking at a single index instead of the data as a whole. There is a version of the STP that uses effective SRH and an effective BWD (Coffer et al. 2019). Based on the idea that elevated supercells cannot produce tornadoes, this revised STP is set to zero whenever the base of the EIL is above the ground. This index would have missed a significant nocturnal tornado that occurred ahead of a warm front at Altus, OK, on 22 February 1975 (Grazulis 1990, p. 565) when the environmental surface temperature and dewpoint were 5°C and 2°C, respectively. The tornado occurred despite the presence of a shallow layer of cold air next to the ground.

Since the thermodynamic factors are not varied in this paper, we set them equal to 1 in the original STP. This provides us with the dynamic STP defined by

$$\mathrm{DSTP} = \frac{\mathrm{SRH}(0{:}1)}{100\ \mathrm{m^2\ s^{-2}}} \times \frac{\mathrm{BWD}}{20\ \mathrm{m\ s^{-1}}} \tag{10}$$

The environment supports supercells when BWD > 20 and mesocyclones when SRH(0:1) exceeds 100 so, given unstable thermodynamic stratification and storm initiation, the threat of significant tornadoes increases with increasing DSTP in excess of one. Because BWD is independent of storm motion, DSTP (like SRH) decomposes into separate parts that depend on mean wind and propagation. Inserting (4) into (10) yields

$$\mathrm{DSTP} = \frac{\mathrm{BWD}}{2000}[\mathrm{MRH}(0{:}\,1) + \mathrm{PH}(0{:}\,1)]. \tag{11}$$

DSTP depends only on the storm motion vector, BWD and the lowest 1 km of the hodograph. DSTP increases as the cube of the scale factor, Δ^3, if propagation is made scale invariant as suggested in section 4.

Since propagation is linked to rotation, the parameter DTSP that predicts significant tornadoes should not be insensitive to propagation in tornado situations. However, this is not generally the case because of the way storm motion is predicted. It turns out that DTSP is determined mainly by the mean-wind term in (11). From (9), we see that the propagation helicity PH(0:1) is practically zero when **S**(0:1) is nearly perpendicular to **S**(0:6). In Brown's (1993) feature-preserving composite SR supercell hodograph (see his figure 5), **S**(0:1) is indeed orthogonal to **S**(0:6). Other examples are the "bent hodographs" of Fig. 1 and section 5. These are straight apart from a right-angle bend at 1 km AGL. Because helicity is twice the area swept out by the storm-relative wind vector (DJBF90), contours of 0-1 km helicity as functions of storm motion, the magenta lines in Fig. 1, are parallel to **S**(0:1). According to

352 the Bunkers method, storms propagate away from the mean wind along the black line in Fig.
353 1, which is the line normal to **S**(0:6) through the tip of the mean-wind vector. Because the
354 line is almost parallel to the magenta lines and the mean wind is far from the 0-1 km leg of
355 the hodograph, the orange area is only slightly larger than the green area. Hence, the 0 to 1
356 km propagation helicity is small compared to MWH(0:1), and the DSTP paradoxically is
357 insensitive to propagation. Other examples of hodographs for which this is true are the
358 semicircular ones in section 6.

359

360 **6. Helicity profiles in proximity to violent tornadoes**

361 We now examine the vertical profiles of helicity and its parts in the environments of two
362 violent tornadoes. The first case (labeled the OK case) is the Sheppard Air Force Base, TX
363 tornado of 3 April 1964 (Charba and Sasaki 1971), which occurred around 1445 CST and had
364 a path length of 9 km (Grazulis 1990, p. 444). This was the only significant tornado in Texas
365 and Oklahoma on this afternoon. The storms on this day split into long-lived RM and LM
366 supercells. Figure 3a shows a proximity hodograph, which is the average of two soundings
367 taken at Ft Sill, OK (70 km to the north of the track) at 1600 and 1720 CST (Charba and
368 Sasaki 1971, their figure 11). The hodograph is almost straight from 0.6 to 7 km. The BWD
369 is 38.3 m s^{-1}.

370 The other case (the NC case) is the Raleigh, NC tornado of 28 November 1988. This
371 violent tornado occurred around 0100 EST, and travelled at 22 m s^{-1} along a path 133 km
372 long (Grazulis 1990, p. 679). The proximity hodograph is from the operational sounding
373 from Greensville, NC, 115 km to the east of Raleigh, at 0600 UTC (0100 EST). The BWD is
374 36.2 m s^{-1}. This case is a good example of a hodograph that resembles a semicircle from the
375 surface to mid-troposphere (Fig. 4a). Composite tornado-proximity hodographs suggest that
376 almost straight hodographs are more common than highly curved ones. However, this
377 conclusion is biased because averaging reduces the directional shear in the lowest 3 km
378 (Brown 1993). While the average of two straight hodographs is always a straight hodograph,
379 the average of two semicircular hodographs is almost always a hodograph with less curvature
380 (Davies-Jones 2003b).

381 In both cases, there are rapid increases in GRH (Figs. 3b, 4b), which are due to the
382 ground-relative wind increasing and veering with height. Considerable warm advection
383 would be indicated *if* the winds were geostrophic. SRH values are high for both

environments. The SRH density (the slope of the SRH curve) is greatest in the lowest 1 km, but is still significantly positive further aloft. The MWH curve is close to the SRH curve in the lowest 1 km, but levels out above 1 km as the as the difference between the wind and the mean wind gets smaller. In the OK case, the left-mover helicity (LMH) is positive below 1 km, negative above it, and its magnitude is much less than that of the SRH. The DSTP for the left-moving supercell is positive (+0.54) even though its updraft was rotating anticyclonically. This suggests that the SRH should be computed over a deeper layer, e.g., 0 to 2 or 3 km (Fig. 3b), for SRH and DSTP to correctly represent the direction of updraft rotation.

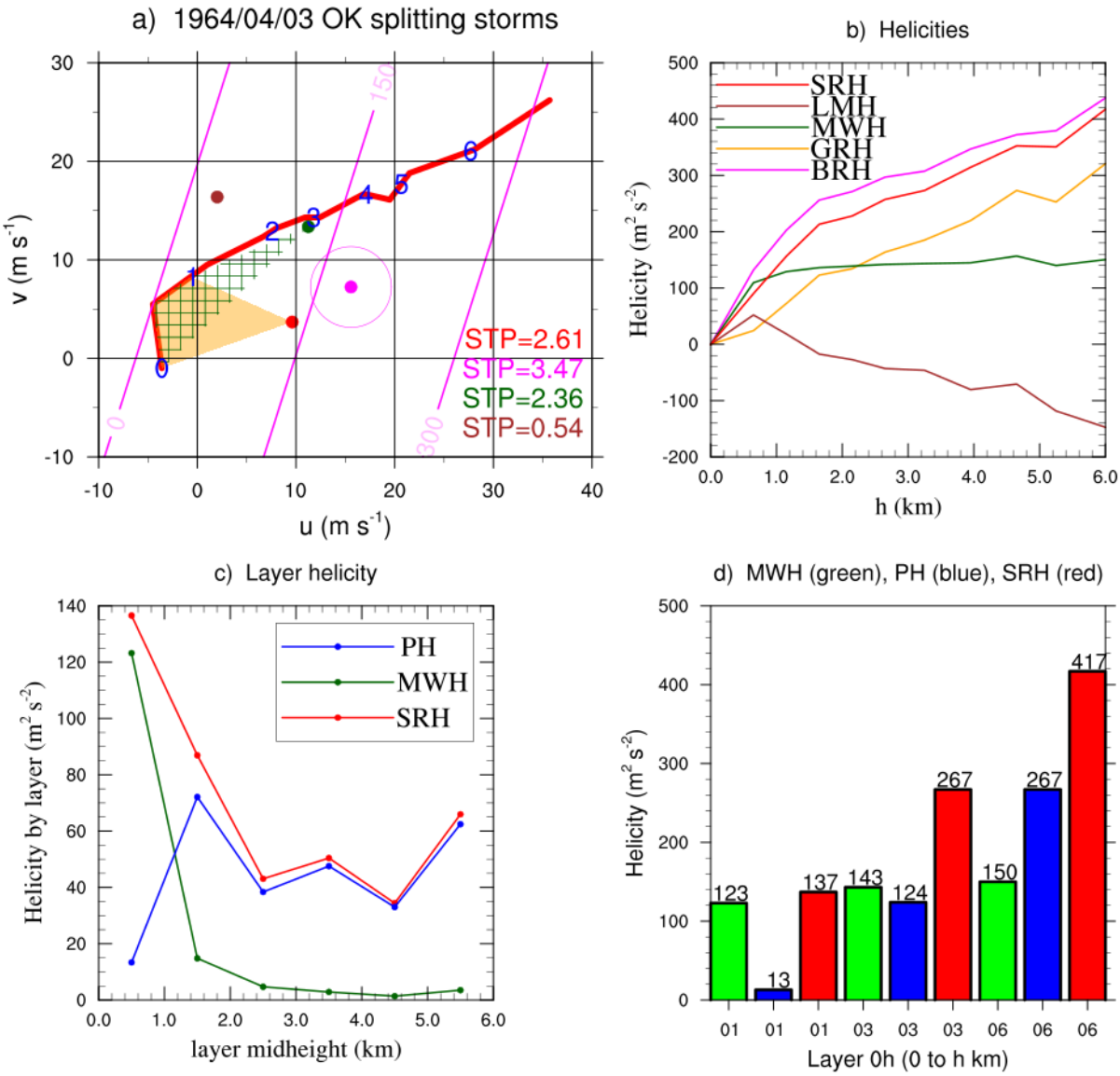

FIG. 3. a) The environmental hodograph for SW Oklahoma on 3 April 1964. The blue numbers along the curve are the heights of the winds in km AGL. The red, brown, and green dots denote the

observed motions of the RM and LM supercells, and the mean wind, respectively. The magenta dot identifies the Bunkers storm motion and the circle around it depicts its mean absolute error. The colored DSTP values are for the observed LM and RM motions (brown and red), and for hypothetical storms moving with the predicted motion (magenta) and the mean wind (green). The areas associated with MWH(0:1) and SRH(0:1) for the RM supercell are filled in with green hatching and orange. The magenta lines are the 0, 150 and 300 contours of SRH(0:1) as a function of observed storm motion (hodograph is from Charba and Sasaki, 1971). b) Storm-relative and ground-relative helicity profiles from 0 to *h*. The storm-relative helicities are for the observed SR and SL supercells (SRH and LMH, respectively), and hypothetical storms that move with the mean wind (MWH) and with the Bunkers predicted motion for the right mover (BRH). c) Layer (0-1, 1-2, …, 5-6 km) values of storm-relative helicity (SRH) and propagation helicity (PH) for the SR supercell. Values are plotted at the mid heights of the layers, e.g., SRH(0:1) is plotted at 0.5 km. d) Bar chart showing the mean-wind helicity (MWH), propagation helicity (PH), and the SRH for layers with bases at the surface and tops at 1, 3, and 6 km. The helicities for elevated layers can be obtained by subtraction [e.g., SRH(1:6) = SRH(0:6) – SRH(0:1)].

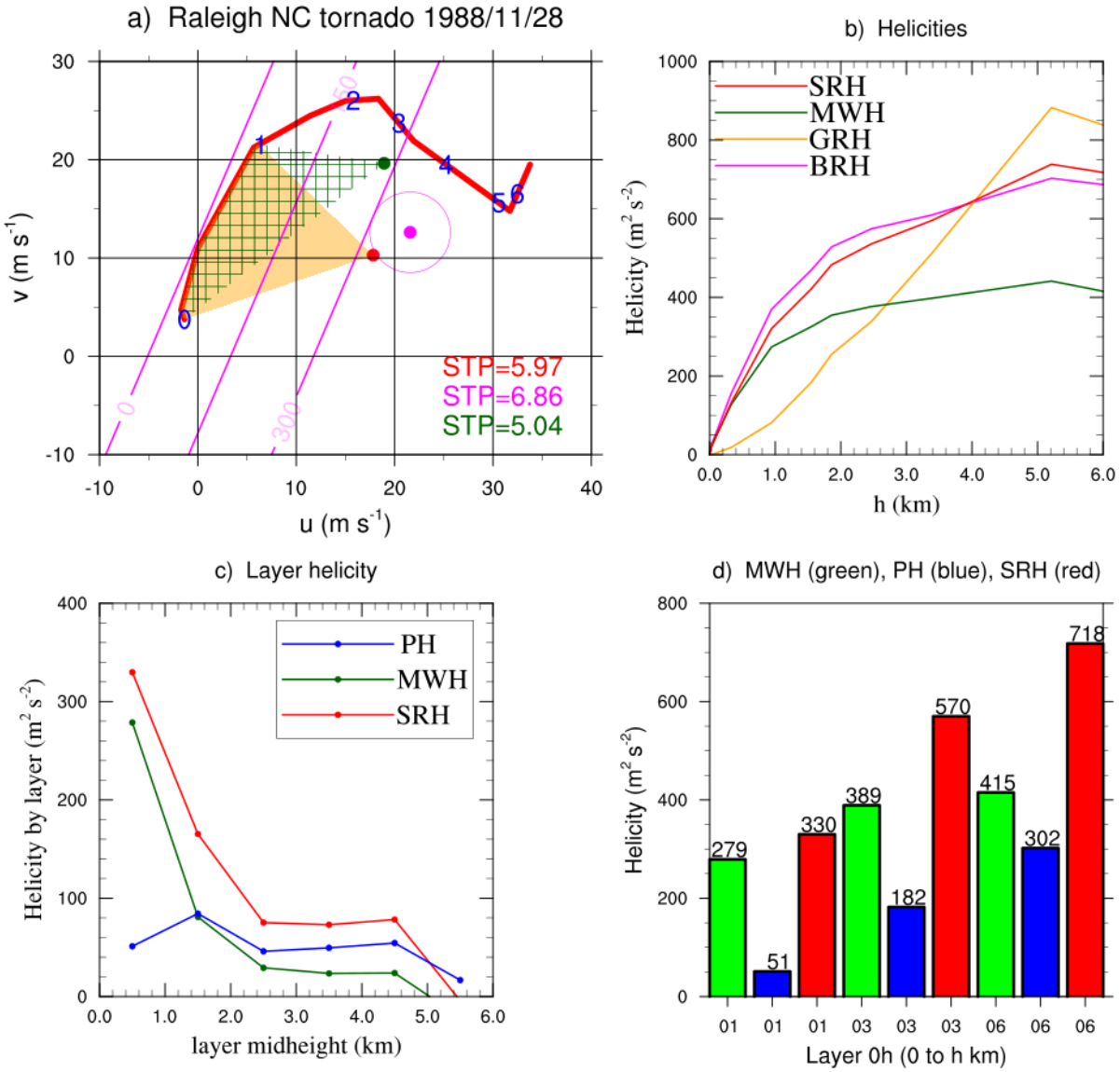

FIG. 4. The environment of the long-track Raleigh, NC tornado on 28 November 1988. The details are the same as in Fig. 3 except the left-moving supercell is absent.

Figures 3c and 4c show the helicities in 1 km thick layers from 0-1 up to 5-6 km. In the lowest 1 km of the environment, almost all of the SRH is comprised of MWH while above 1 km the SRH is due predominantly to PH. The layer with by far the most SRH is the 0-1 km layer where the PH is small.

The bar charts in Figs. 3d and 4d show that for the 0-1 km and 0-3 km layers (and even the 0-6 km layer in the NC case), MWH exceeds PH. Weisman & Rotunno (2000, p. 1471) state that, in the helicity-streamwise vorticity viewpoint, "a storm generates rotation by virtue of propagation". However, most of the helicity of parcels in the lowest one or three kilometers (the ones with the most CAPE) is mean-wind helicity, not propagation helicity. If the updraft did not propagate at all, it would still rotate.

On both days, the supercells are moving considerably slower than predicted. The error is 7 m s^{-1} in the OK case (Fig. 3a) and 5 m s^{-1} in the NC case (Fig. 4a). The predicted motions produce SRH values that are too large.

Despite BWD being nearly the same in both cases, the SRH is much larger for the NC case than in the OK case (c.f. Figs. 3d and 4d). This is due to greater shears and to storm motion being further off the hodograph (Figs. 3a and 4a). The 0-1 km MWH is much larger in the NC case (see Figs. 3c and 4c) due mainly to the greater low-level (compare Figs. 3a and 4a). The surface vorticity is practically streamwise in the OK case and less so in the NC case.

In the next sections, we investigate the properties of some idealized hodographs with simple shapes. The forms are straight lines, straight on either side of a right-angle bend at z = 1 km, and semicircular. For hodographs of the same size and shape, the SRH profile and the DSTP depend on how the curve parameter *z* is distributed along the hodograph curve (McCaul and Weisman, 2001; Markowski and Richardson, 2014). Therefore, we vary the shear magnitude with height. In most cases, insightful formulas exist for the mean wind, the predicted storm-relative wind, various helicities and DSTP (appendix).

7. Purely straight hodographs

For a perfectly straight hodograph, the mean wind lies on the hodograph and the MWH is zero. When the storm motion vector **c** also lies on the hodograph, the SRH density is zero, indicating zero covariance between updraft and vertical vorticity even though vertical velocity and vertical vorticity both may be large. Simulations confirm that, in unidirectional shear, initial storms (prior to splitting into RM and LM storms) are not supercells (Rotunno and Klemp, 1985). Updrafts rotate as a whole only by propagating off the hodograph.

In unidirectional shear,

$$\mathrm{SRH}(0\!:\!h) = 7.5|\mathbf{S}(0\!:\!h)| \tag{12}$$

for the right-moving supercell. The SRH is independent of where the mean wind lies on the hodograph. It is due entirely to storm propagation off the straight hodograph, and has a simple explanation. Recall that SRH(0:*h*) is twice the area swept out clockwise from 0 to *h* by the predicted SR wind vector. For a straight hodograph, the area is a triangle with base |**S**(0,*h*)| and height 7.5. In Figs. 5a and b, the SRH from 0 to 1 km is twice the area of the orange shaded triangle whose base lies along the hodograph from 0 to 1 km and whose height is the perpendicular distance from the predicted storm motion (the magenta dot) to the hodograph. The storm motion can lie anywhere along a line parallel to the hodograph and at a distance $\sigma|\mathbf{S}(0{:}6)|$ from it without affecting the SRH. For a straight hodograph

$$\mathrm{DSTP} = \frac{7.5|\mathbf{S}(0\!:\!1)||\mathbf{S}(0\!:\!6)|}{2000} = \frac{7.5\ \mathrm{BWD}}{2000}|\mathbf{S}(0\!:\!1)|. \tag{13}$$

For demonstration straight hodographs, we employ

$$u(z) = u_0 + \left[\frac{6}{5}u(1) - \frac{1}{30}u(6)\right]z + \left[\frac{1}{30}u(6) - \frac{1}{5}u(1)\right]z^2, v = v_0 \tag{14}$$

where z is in km, $u_0 = 0$, $v_0 = 8$. The shear magnitude is

$$|\mathbf{S}| = \left[\frac{6}{5} - \frac{2}{5}z\right]u(1) + \left[\frac{1}{15}z - \frac{1}{30}\right]u(6) \tag{15}$$

and its derivative is

$$\frac{d|\mathbf{S}|}{dz} = \frac{u(6) - 6u(1)}{15}. \tag{16}$$

The hodograph curves are parallel to the u-axis with $u(0) = 0$ and $u(6) = 37.5$ to maintain a constant BWD of 37.5. For the hodograph with constant shear. $u(1) = u(6)/6 = 6.25$. For a hodograph with declining shear that remains positive for $0 < z < 6$, we choose $u(1) = 10.5$.

The SRH(0:1) in Figs. 5a and b are twice the area of the orange triangle or 7.5u(1). More generally, SRH(0:h) = 7.5u(h). The DSTP is 7.5u(1)u(6)/2000.

Figs. 6a and b show the relative helicity for the two straight hodographs. The helicity density (the slope) is constant in the constant-shear case, and is largest at the ground when the shear declines. The helicity in 1 km thick layers between n and n+1 km (where n is a whole number between 0 and 5) is

$$\begin{aligned} \mathrm{SRH}(n{:}\,n+1) &= \mathrm{SRH}(0{:}\,n+1) - \mathrm{SRH}(0{:}\,n) \\ &= 7.5[u(n+1) - u(n)]. \end{aligned} \tag{17}$$

In the constant-shear case, $u(n+1) - u(n) = 6.25$ so the SRH of each layer = 6.25x7.5 = 47 and the DSTP = 47x37.5/2000 = 0.88. In the declining-shear case, SRH(n:n+1) declines linearly with n as shown in Fig. 6b. Since the BWD is the same in both cases, the declining shear case has a greater SRH(0:1), 79, and a greater DSTP, 1.48.

For unidirectional shear, all the helicity is due to propagation, and SRH(0:1) and the DSTP are independent of the mean wind. They only depend on the length of the hodograph from 0 to 6 km and on the 0-1 km length. We next consider the quite different situation of bent hodographs where change in direction of the shear vector plays an important role in the low-level helicity and DSTP.

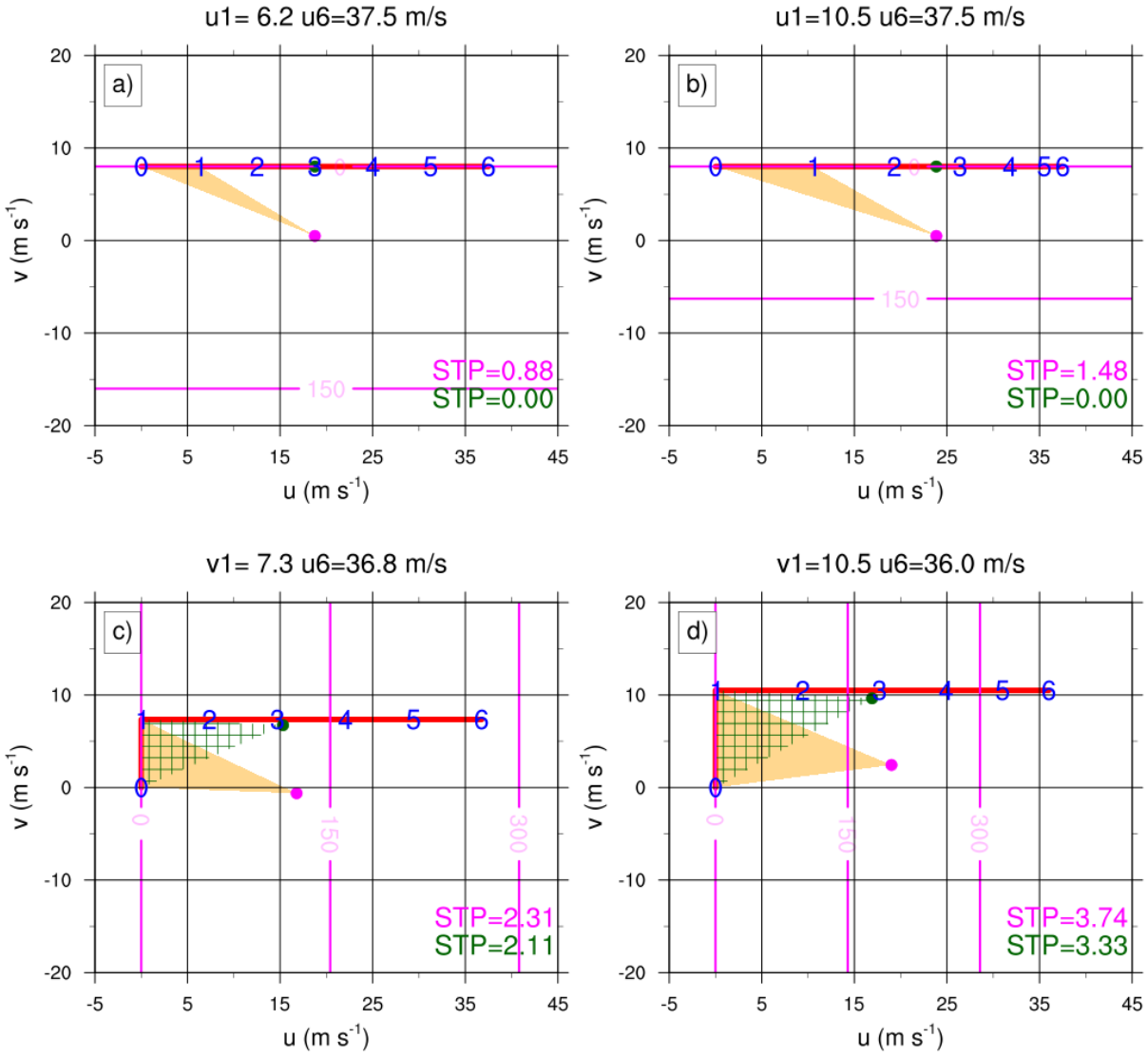

FIG. 5. Examples of idealized straight hodographs with and without bends. Cases a) and b) are straight hodographs with constant shear and declining shear magnitude, respectively, and cases c) and d) are similar but with right-angle bends at 1 km AGL. The blue numbers along the hodographs (red lines) are the heights of the winds in km AGL. The magenta dot depicts the Bunkers storm motion. The green dot marks the mean wind. The area associated with SRH(0:1) for the RM supercell is filled in orange. The contours of SRH(0:1) are evenly spaced straight magenta lines with a contour interval of 150. The zero contours (not shown) are lines through the 0-1 km segments of the hodographs. The area associated with MWH(0:1) is filled with green hatching. The BWD is the same (37.5 m s^{-1}) in all these hodographs. The color of the DSTP value matches the color of the motion vector used in its evaluation.

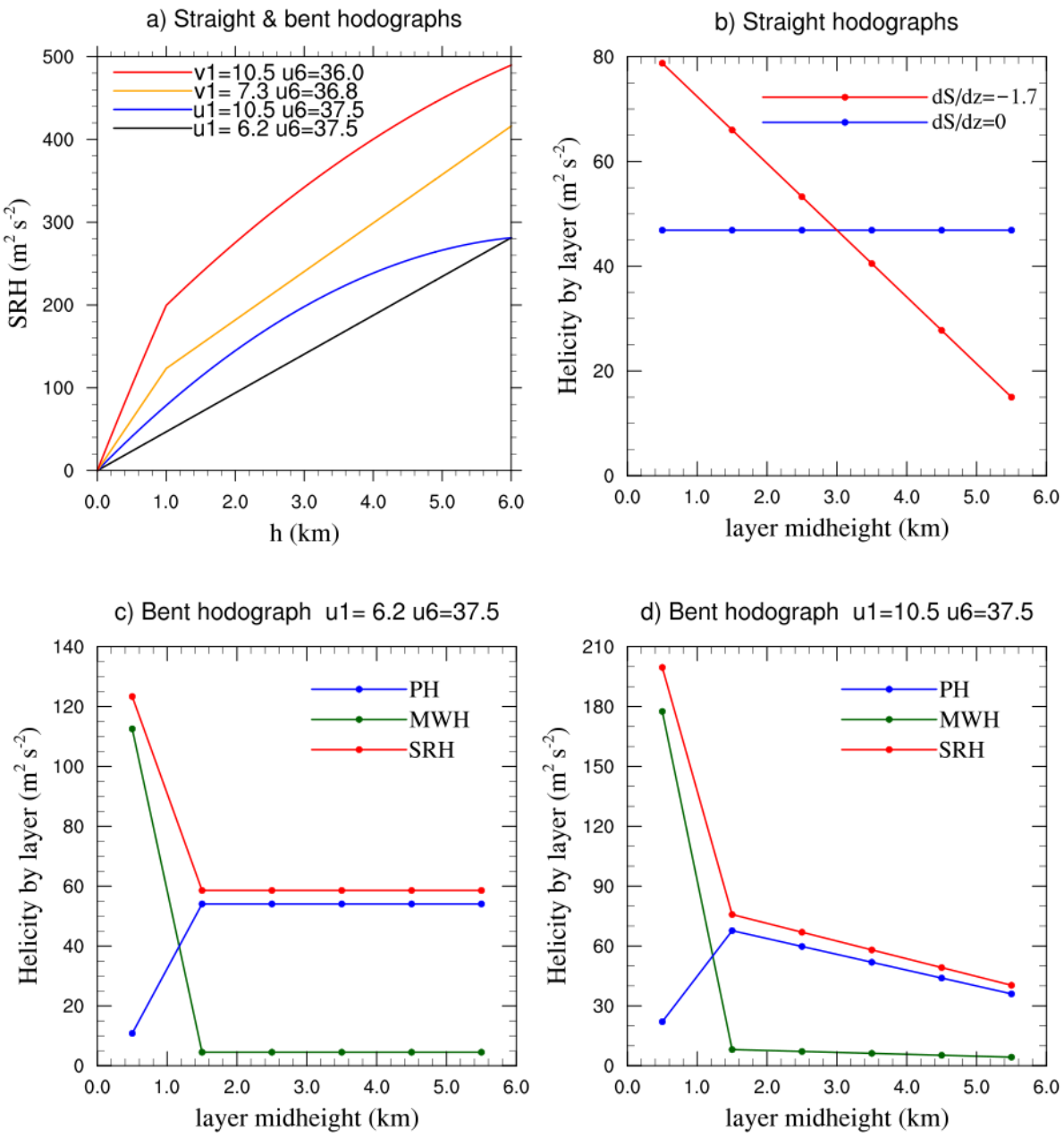

502

503 FIG. 6. a). SRH(0:*h*) for the straight and bent hodographs shown in Fig. 5. b) SRH for the
504 constant ($d|\mathbf{S}|/dz$ =0) and declining ($d|\mathbf{S}|/dz$ = –1.7 x 10^{-3} km^{-1} s^{-1}) unidirectional shear cases. The
505 data points are plotted at the layer mid heights, n + 0.5 km of the layers (where n is whole), and are
506 connected by lines. For purely straight hodographs, MWH is identically zero and PH is equal to SRH.
507 c) SRH, MWH, and PH per 1 km thick layers for the hodograph in Fig. 5c. d) As in c) but for the
508 hodograph in Fig. 5d.

509

510 **8. Hodographs with right-angle bends**

511 For simplicity we consider hodographs shaped like ↦ with a right-angle bend at a fixed
512 height, z = 1 km, and again assume a linear variation of vertical wind shear with height.

513 Without loss of generality, the 'bent' hodograph is translated and rotated so that the surface
514 wind is zero and **S**(1,6) is parallel to the *u*-axis.

515 The wind formulas for these hodographs are

516 $$u(z) = 0, v(z) = \left[\frac{7}{6}v(1) - \frac{1}{30}u(6)\right]z + \left[\frac{1}{30}u(6) - \frac{1}{6}v(1)\right]z^2 \qquad (18)$$

517 for $z \leq 1$ and

518 $$u(z) = \left[\frac{7}{6}v(1) - \frac{1}{30}u(6)\right](z-1) + \left[\frac{1}{30}u(6) - \frac{1}{6}v(1)\right](z^2-1), v(z) = v(1) \qquad (19)$$

519 for $z > 1$.

520 The two free parameters, $v(1)$ and $u(6)$, are chosen as follows. Firstly, we impose the
521 condition $[v^2(1) + u^2(6)]^{0.5} = 37.5$, which makes the BWD the same as for the straight
522 hodographs. Secondly, we either constrain the shear magnitude to be constant with height or
523 we make the 0-1 km shear magnitude the same as in the declining unidirectional shear case.
524 The first alternative makes $v(1) = u(6)/5 = 7.35$ and $u(6) = 36.75$, resulting in the hodograph
525 in Fig. 5c). The second alternative makes $v(1) = 10.5$, $u(6) = 36$, and produces the hodograph
526 in Fig. 5d, which is roughly comparable to the OK case in Fig. 2a.

527 From Fig. 6a, we see that the predicted helicities SRH(0:*h*) for the bent hodographs are
528 greater at all heights than for the straight hodographs. The bent hodograph with the shear
529 concentrated at the ground has the largest helicities. Introducing the bend in the hodograph
530 has two effects. First, the mean wind lies slightly to the right of the hodograph curve instead
531 of on it. Second and far more importantly, the bend in the hodograph has caused a much
532 larger orange area compared to that for the comparable straight hodograph (see Fig. 5). The
533 base of the orange 0-1 km helicity triangle is turned 90° and so the mathematical height of
534 this triangle is the distance from the predicted motion vector to the southerly leg of the
535 hodograph rather than the smaller distance from the motion vector to a westerly leg as in the
536 unidirectional case (Fig. 6). Thus, the MWH(0:1), the green hatched area, becomes large
537 while the MWHs of all the higher layers remains small. In the lowest 1 km, the MWH
538 dominates the PH as evident in Figs. 6c and 6d. SRH(0:1) is hardly affected by propagation
539 off the hodograph. This is in marked contrast to a unidirectional hodograph, for which the PH
540 is the entire SRH for all layers. The bent hodograph is not just a minor variation of a straight
541 hodograph. Even if there were no propagation off the hodograph, there would still be storm-

relative helicity. From a helicity viewpoint, propagation off the hodograph is not needed for a storm to rotate.

For layers based at 1 km and above, PH dominates MWH (Figs. 6c, d). This physics is not included in the DSTP, which involves only the 0-1 km SRH. PH does make a substantial contribution to SRH(0:3) (Fig. 6a).

Next, we investigate a completely different shape of hodograph, the semicircle from 0 to 6 km.

9. Semicircle hodographs

We replicate semicircular hodographs by letting

$$u(z) = u_c - A\cos\phi(z), v(z) = v_c + A\sin\phi(z),$$
$$\phi(z) = \frac{\pi}{36z_0 - 6z_0^2}[(18 - z_0^2)z + (z_0 - 3)z^2]. \quad (20)$$

where z is height in km, the center of the semicircle is at (u_c,v_c) = (10,0), its diameter is A = 17.5, its base is along the u-axis, and z_0 is the height in km at which v is a maximum. When z_0 = 3 km, the rate that the wind veers with height is constant. The shear vanishes at the ground for z_0 = 4.24 km and at 6 km for z_0 = 1.76 km. For demonstration purposes, we use z_0 = 1.76, 3, and 4.24 km. The hodographs and the helicity areas are illustrated in Fig. 7. The case z_0 = 1.76 km (Fig. 7a) roughly resembles the Raleigh, NC hodograph in Fig. 4a. For semicircle hodographs, SRH(0:1) and DSTP calculated using the predicted storm motion are only slightly greater than the corresponding quantities calculated with the mean wind (Fig. 7a). The quantities are greatest for the case with the most shear near the ground.

Since the BWD = 35, all the environments should support supercells storms. In the z_0 = 4.24 case however, the small values of low-level SRH (Fig. 8a) and DSTP (Fig. 7) portend little updraft rotation. Because BWD is simply the vector wind difference between 0 and 6 km, it fails to distinguish between low-level and mid-level shear and hence misrepresents the supercell potential when the shear is predominantly in mid-troposphere. For z_0 = 3 and 1.76, all the parameters predict supercells. Of all the idealized hodographs considered in this paper, the semi-circle one with very large values of shear near the ground (z_0 = 1.76) has the largest DSTP by far (Figs. 7).

571 The helicity profiles for the three cases are shown in Fig. 8a. SRH(0:6) is nearly the same
572 but SRH(0:3) increases greatly with the amount of low-level shear. 'Long' hodographs that
573 are 'short' near the ground are unfavorable for helical storms.

574 Figs. 8b-d present the MWH and PH by layer for the three semi-circle hodographs. For
575 these hodographs, the propagation helicity equals the MWH for one or two layers and
576 otherwise is a small fraction of the MWH. For the z_0 = 3 and 1.76 hodographs, MWH (0:1),
577 MWH(0:3), and MWH(0:6) are all large so updrafts would still be helical even if they did not
578 propagate. Propagation helicity just makes these updrafts slightly more helical.

579

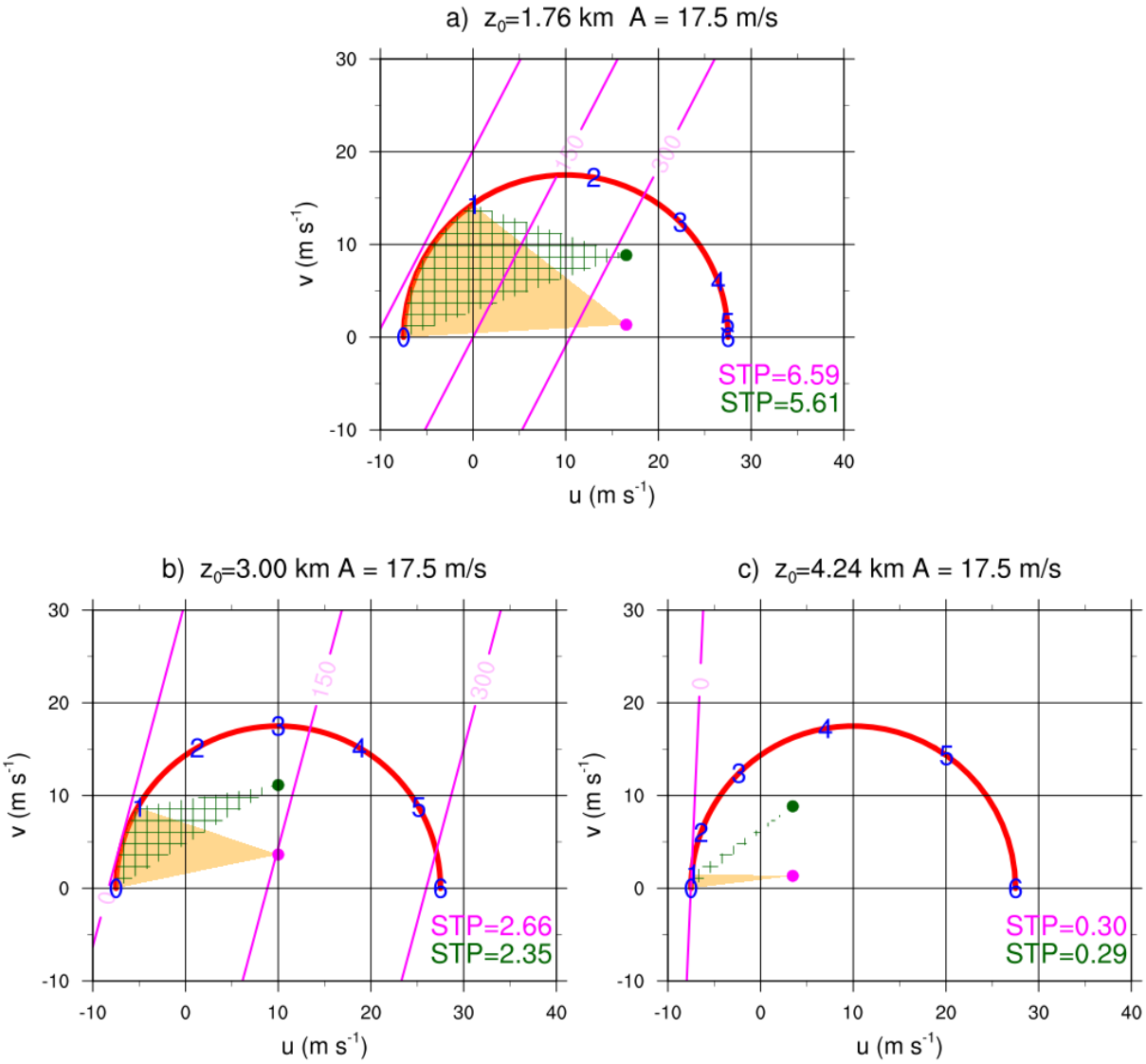

580

581 FIG. 7. As in Fig. 5, but for semi-circle hodographs with the same diameter 2*A* = 35 (=BWD) and
582 different z_0. In a) z_0 = 1.76 km and the shear magnitude is largest at the ground and declines with

height. In b) z_0 = 3 km and the shear magnitude is constant. In c) z_0 = 4.24 km and the shear is very weak near the ground and strong in mid-troposphere.

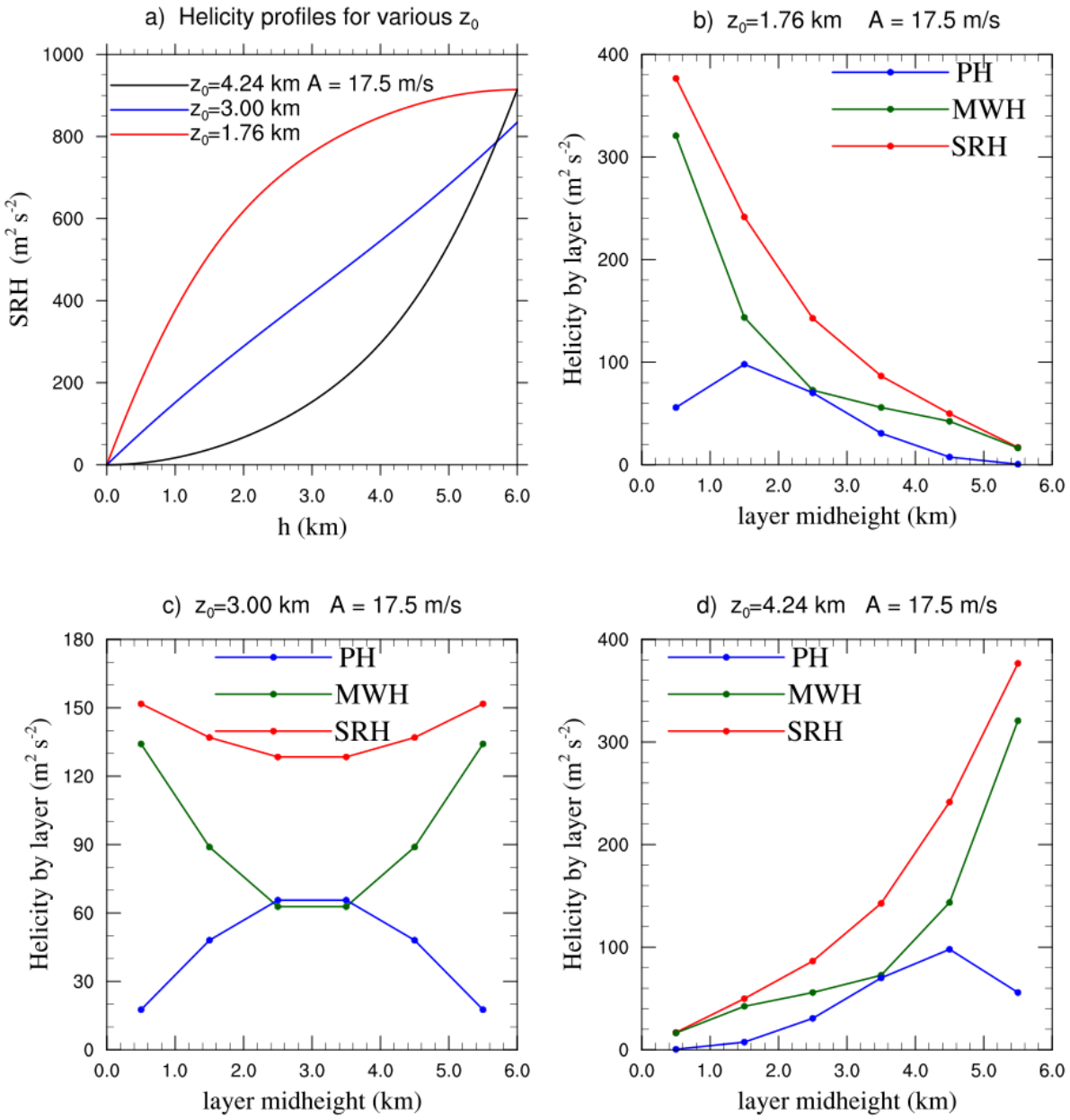

FIG. 8. a) SRH(0:*h*) for the semi-circular hodographs with the same diameter but different z_0. The black, blue, and red curves are for the cases where the shear magnitude increases, is constant, and decreases with height, respectively. b) The layer helicities SRH(*n*:*n*+1), MWH(*n*:*n*+1), and PH(*n*:*n*+1) for the semi-circular hodograph with declining shear magnitude. The data points are plotted at the layer midheights, *n* + 0.5 km. c) As in b), but for the semi-circular hodograph with constant shear magnitude. d) As in b) but for the semi-circular hodograph with shear magnitude increasing with height. This panel is the mirror image of panel b) in the line *z* = 3 km.

10. Intercomparison of hodographs

The bar charts in Fig. 9 summarize the 0-1, 0-3 and 0-6 km SRH, MWH, and PH for the right-moving supercells in the sample of hodographs used herein. The BWDs vary slightly from 35 to 38.3, and favor supercell formation. Also shown are the DSTP based on the predicted storm motion and its parts due to the mean wind and propagation. The helicities and DSTP vary with hodograph shape and variation of shear with height.

The idealized hodographs vary in shape from straight (leading U in the case identifier in Fig. 9) to bent (B) to semi-circular (S) and in the shear distribution (trailing H, E, and L respectively indicate that the magnitude of shear is greatest at 6 km, constant, and greatest at the ground). As stated previously, the OK and NC environmental hodographs respectively match the BL and SL idealized ones one quite well. Purely straight hodographs are rare in tornado situations because the combination of Ekman veering and warm-air advection causes the shear vector to turn considerably in the lowest 1 km.

Given the same type of shear distribution and BWD, the DSTP and implied tornado threat varies with the shape of the hodograph. The risk is low for straight ones, moderate for bent ones, and great for semi-circular. For hodographs with the same shape and 0-6 bulk shear, the threat increases as the shear distribution changes in type from H to E to L. The rankings from least to greatest threat based on either SRH(0:1) or DSTP are SH, UE, UL, BE, SE, BL, SL. If the ranking is based instead on SRH(0:3), the only changes are that UE and SH swap places as do SE and BL. By these measures, SL is the most dangerous hodograph, followed by BL or SE.

From (9), PH(0:h) equals 7.5 times the component of $\mathbf{S}(0{:}h)$ in the direction of $\mathbf{S}(0{:}6)$. Hence, PH(0:6) equals 7.5 BWD and ranges from 262 to 287. Since $\mathbf{S}(0{:}1)$ is much smaller than $\mathbf{S}(0{:}6)$ and is often in a different direction, PH(0:1) is small compared to PH(0:6). In Fig. 9, it is less than 101 for every hodograph. PH(0:3) is intermediate between PH(0:1) and PH(0:6). Propagation generally makes the surface environmental vorticity more streamwise for the right-moving supercell and less streamwise for the left mover if there is one (Figs. 3a, 4a, 5, 7).

For straight hodographs, MWH is zero. For all other hodographs in the set, MWH(0:1) far exceeds PH(0:1). For the bent hodographs, PH(0:3) and MWH(0:3) are comparable and PH(0:6) exceeds MWH(0:6). In the semicircle cases, MWH is much larger than PH for all surface-based layers.

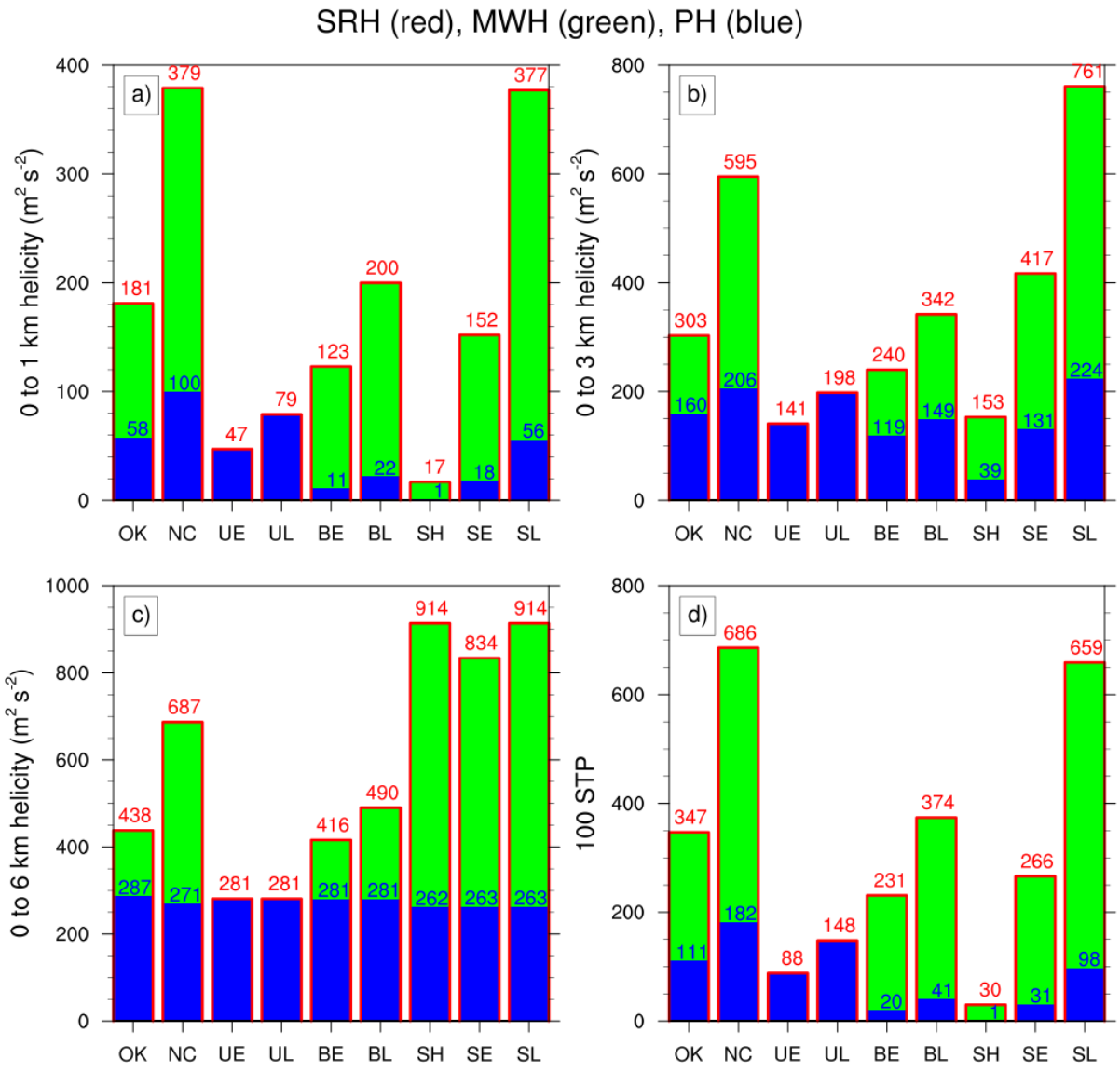

FIG. 9. Bar charts of helicities and the DSTP for each hodograph in this paper. All SRH, PH and DSTP values in this figure are calculated using the storm motion predicted by the Bunkers' method. Apart from the two real soundings OK and NC, the first letter of each case identifies the hodograph shape (U for unidirectional shear, B for bent, or S for semi-circle) and the second letter labels the variation of shear magnitude (H for greatest shear at 6 km, E for equal shear magnitude, and L for greatest shear at surface). The hollow red bars topped by red numbers, the filled blue bars topped with blue numbers, and the green fillings depict the SRH, PH, and MWH (= SRH – PH) for each case. In a), b), c), the helicities are for 0-1, 0-3, 0-6 layers. In d) 100 DSTP is plotted with similar partitions.

11. Summary

We noted that the propagation speed should be proportional to the bulk wind difference (BWD) between 0 and 6 km AGL in order to make the predicted (Bunkers) storm motion scale invariant for similar hodographs of different sizes. We stuck with the fixed propagation speed, 7.5 m s^{-1}, because it is the one in routine use and because there was little variation in BWD in the sample set of hodographs. These BWDs are far into the supercell range.

We then examined two very different hodographs that were obtained in close proximity to violent tornadoes. One was nearly straight from 1 to 7 km AGL with a bend at 1 km and the other approximated a semi-circle from 0 to 5 km AGL. In addition, we investigated the tornado potential of idealized hodographs of different shapes (straight, bent, and semi-circular) with different distributions of shear magnitude with height.

To rank the hodographs in terms of tornado risk, we use the DSTP. This is the dynamic part of the significant tornado parameter, which is a widely used tornado forecast parameter. DSTP is the product of SRH(0:1) and BWD divided by 2000. Since the BWD is nearly constant for our set of hodographs, the DSTP is proportional to the SRH(0:1). In tornado environments, SRH(0:1) is large, and SRH(0:*h*) increases with height up to at least 5-6 km, albeit at a rate that decreases with *h* above 1 km.

Bent hodographs are more favorable for tornadoes than straight ones because significant turning of the shear in the lowest kilometer greatly increases low-level SRH. The tornado threat is greatest with semicircle hodographs. Concentration of the wind shear near the ground greatly increases the tornado potential for all the hodographs.

To evaluate the role of propagation in tornadogenesis, we decomposed the storm-relative helicity in a layer from $z = b$ to h km, SRH(b:h), into the sum of the mean-wind helicity, MWH(b:h), and a propagation helicity PH(b:h) where MWH is the SRH for a storm moving with the mean wind and PH ≡ SRH − MWH is the helicity due to propagation. The DSTP similarly breaks into mean-wind and propagation parts.

For purely straight hodographs, the MWH is zero and the modest DSTP score is due solely to propagation. For bent and semicircular hodographs, MWH dominates PH near the ground. Because the shear in the lowest kilometer is nearly perpendicular to the 0-6 km bulk shear, the low-level PH is small compared to MWH and contributes little to the substantial DSTP scores of these hodographs. Consequently, high DSTP scores are insensitive to the Bunkers at al. propagation velocity.

672 Storm-relative helicity often is incorporated into the significant tornado parameter
673 through SRH(0:1) or SRH(0:0.5) factors. This causes propagation to be underrepresented in
674 STP. For example, in the OK case, SRH(0:1) is positive instead of negative for the left-
675 moving storm with an anticyclonically rotating updraft and negative vertical helicity. Using
676 SRH(0:2) instead would result in STP having the correct sign for the left-moving storm and
677 in a larger propagation contribution to STP for bent hodographs. However, the propagation
678 helicity is much smaller than the large mean-wind helicity present at all heights for the
679 semicircle hodographs with declining shear magnitude (Figs. 8, 9). This indicates that storm
680 propagation away from the mean wind is not essential for updraft rotation in some
681 environments, which just happen to be the ones with the largest threat.

682

683 *Acknowledgments.*

684 An earlier version of this paper was presented at the 11th European Conference on Severe
685 Storms (Bucharest, May 8-12, 2023). I am grateful to the European Severe Storms
686 Laboratory for waiving my registration fee.

687

688 *Data Availability Statement.*

689 The data are in the public domain.

690

691 APPENDIX

692 **Formulas for some properties of the idealized hodographs**

693 The following analytically derived formulas for the mean wind, the predicted storm-
694 relative wind, various helicities and DSTP provide generality as well as useful checks on the
695 code.

696 For the straight hodographs defined by (14), the most relevant quantities are given by

697 $$\mathrm{BWD} = u(6), \tag{A1}$$

698 $$\bar{\mathbf{v}} = [1.2u(1) + 0.3u(6)]\mathbf{i} + v_0\mathbf{j}, \tag{A2}$$

699 $$\mathbf{c}_{\mathrm{RM}} = \bar{u}\mathbf{i} + [v_0 - 7.5]\mathbf{j}, \tag{A3}$$

700 $$\mathrm{MWH}(0\colon z) = 0, \mathrm{SRH}(0\colon z) = \mathrm{PH}(0\colon z) = 7.5u(z), \tag{A4}$$

$$\mathrm{DSTP} = \frac{7.5u(1)u(6)}{2000}. \tag{A5}$$

For the bent hodographs described by (18) and (19), the formulas are

$$\mathrm{BWD} = [u^2(6) + v^2(1)]^{0.5}, \tag{A6}$$

$$\bar{\mathbf{v}} = \frac{65u(6) + 125v(1)}{216}\mathbf{i} + \left[\frac{199}{216}v(1) - \frac{1}{1080}u(6)\right]\mathbf{j}, \tag{A7}$$

$$\mathbf{c}_{\mathrm{RM}} = [\bar{u} + \sigma v(1)]\mathbf{i} + \big(\bar{v} - \sigma u(6)\big)\mathbf{j}, \tag{A8}$$

where σ= 7.5/BWD from (8). The helicities in 1 km thick layers between n–1 and n km and DSTP are

$$\begin{aligned} \mathrm{MWH}(0\text{:}\,1) &= \bar{u}v(1), \\ \mathrm{MWH}(n-1\text{:}\,n) &= [u(n) - u(n-1)][v(1) - \bar{v}] \text{ for } n = 2,3,4,5,6 \end{aligned} \tag{A9}$$

$$\begin{aligned} \mathrm{PH}(0\text{:}\,1) &= \sigma v^2(1), \\ \mathrm{PH}(n-1\text{:}\,n) &= [u(n) - u(n-1)]\sigma u(6) \text{ for } n = 2,3,4,5,6 \end{aligned} \tag{A10}$$

$$\mathrm{DSTP} = \frac{\mathrm{BWD}}{2000}\bar{u}v(1) + \frac{7.5}{2000}v^2(1). \tag{A11}$$

For the semicircle hodographs defined by (20) with constant shear magnitude (z_0 = 3 km),

$$\mathrm{BWD} = 2A, \tag{A12}$$

$$\bar{\mathbf{v}} = u_c\mathbf{i} + \left(v_c + \frac{2A}{\pi}\right)\mathbf{j}, \tag{A13}$$

$$\mathbf{c}_{\mathrm{RM}} = u_c\mathbf{i} + \left(v_c + \frac{2A}{\pi} - 7.5\right)\mathbf{j}, \tag{A14}$$

$$\mathrm{MWH}(0\text{:}\,z) = \frac{\pi}{6}A^2 z - \frac{2}{\pi}A^2\left(1 - \cos\frac{\pi z}{6}\right), \tag{A15}$$

$$\mathrm{PH}(0\text{:}\,z) = 7.5A\left(1 - \cos\frac{\pi z}{6}\right), \tag{A16}$$

$$\mathrm{DSTP} = \frac{A^2}{1000}(0.4383A + 1.005). \tag{A17}$$

There are no simple formulas for semicircle hodographs with other values of z_0.

REFERENCES

723 Brown, R. A., 1993: A compositing approach for preserving significant features in
724 atmospheric profiles. *Mon. Wea. Rev.,* **121,** 874-880.

725 Bunkers, M. J., B. A. Klimowski, J. W. Zeitler, R. L. Thompson, and M. L. Weisman, 2000:
726 Predicting supercell motion using a new hodograph technique. *Wea. Forecasting*, **15**, 61-
727 79.

728 Charba, J., and Y. Sasaki 1971: Structure and movement of the severe thunderstorms of 3
729 April 1964 as revealed from radar and surface mesonetwork data analysis. *J. Meteor. Soc.*
730 *Japan*, **49**, 191-213.

731 Church, C., D. Burgess, C. Doswell, and R. Davies-Jones (editors), 1990: *The Tornado: Its*
732 *Structure, Dynamics, Prediction, and Hazards*, Geophysical Monograph **79**, AGU Press,
733 1993.

734 Coffer, B. E., M. D. Parker, R. L. Thompson, B. T. Smith, and R. E. Jewell, 2019: Using
735 near-ground storm relative helicity in supercell tornado forecasting. *Wea. Forecasting*,
736 **34**, 1417-1435.

737 Coffer, B. E., M. D. Parker, M. C. Coniglio, and C. R. Homeyer, 2025: Supercell
738 environments using GridRad-Severe and the HRRR: Addressing discrepancies between
739 prior tornado datasets. *Wea. Forecasting*, **40**, 1405-1428.

740 Davies-Jones, R. P., 1984: Streamwise vorticity: The origin of updraft rotation in supercell
741 storms. *J. Atmos. Sci.,* **41,** 2991-3006.

742 Davies-Jones, R., 2003a: An expression for effective buoyancy in surroundings with
743 horizontal density gradients. *J. Atmos. Sci.,* **60,** 2922-2925.

744 Davies-Jones, R. P., 2003b: Reply. *J Atmos. Sci*., **60**, 2420-2426.

745 Davies-Jones, R. P., 2004: Growth of circulation around supercell updrafts. *J. Atmos. Sci*., **61**,
746 2863-2876.

747 Davies-Jones, R. P., D. W. Burgess and M. Foster, 1990: Test of helicity as a tornado forecast
748 parameter. *Preprints,* 16th Conf. Severe Local Storms, Kananaskis Provincial Park,
749 Alberta, Amer. Meteor. Soc., 588-592.

750 Droegemeier, K. K., S. M. Lazarus and R. Davies-Jones, 1993: The influence of helicity on
751 numerically modelled storms. *Mon. Wea. Rev.,* **121,** 2005-2029.

752 Esterheld, J. M., and D. J. Giuliano, 2008: Discriminating between tornadic and non-tornadic
753 supercells: A new hodograph technique. *Electronic J. Severe Storms Meteor*., **3** (2), 1-50.

754 Grazulis, T. P., 1990: *Significant Tornadoes 1880-1989. Volume II: A Chronology of Events.*
755 Environmental Films, St. Johnsbury, Vermont, 685 pp.

756 Kreyszig, E., 1972: *Advanced Engineering Mathematics*. 3rd ed. Wiley, 866 pp.

757 Lilly, D. K., 1986: The structure, energetics and propagation of rotating convective storms.
758 Part II: Helicity and storm stabilization. *J. Atmos. Sci.*, **43**, 126-140.

759 Markowski, P. M., and Y. P. Richardson, 2014: The influence of environmental low-level
760 shear and cold pools on tornadogenesis: Insights from idealized simulations. *J. Atmos.*
761 *Sci.*, **71**, 243–275.

762 Markowski, P. M, C. Hannon, J. Frame, E. Lancaster, A. Pietrycha, R. Edwards, and R. L.
763 Thompson, 2003: Characteristics of vertical wind profiles near supercells obtained from
764 the Rapid Update Cycle. *Wea. Forecasting*, **18**, 1262-1272.

765 McCaul, E. W., Jr., 1991: Buoyancy and shear characteristics of hurricane-tornado
766 environments. *Mon. Wea. Rev*., **119**, 1954–1978.

767 McCaul, E. W., Jr., and M. L. Weisman, 2001: The sensitivity of simulated supercell
768 structure and intensity to variations in the shapes of environmental buoyancy and shear
769 profiles. *Mon. Wea. Rev*., **129**, 664–687.

770 Peters, J. M., C. J. Nowotarski, J. P. Mulholland, and R. L. Thompson, 2020: The influences
771 of effective inflow layer streamwise vorticity and storm-relative flow on supercell updraft
772 properties. *J. Atmos. Sci.*, **77**, 3033–3057.

773 Rasmussen, E. N., 2003: Refined supercell and tornado forecast parameters. *Wea.*
774 *Forecasting*, **18**, 530-535.

775 Rotunno, R., and J. B. Klemp, 1985: On the rotation and propagation of simulated supercell
776 thunderstorms. *J. Atmos. Sci.*, **42**, 271–292.

777 Thompson, R. L., R. Edwards, J. A. Hart, K. L. Elmore, and P. Markowski, 2003: Close
778 proximity soundings within supercell environments obtained from the Rapid Update
779 Cycle. *Wea. Forecasting*, **18**, 1243–1261.

780 Thompson, R. L., C. M. Mead, and R. Edwards, 2007: Effective storm-relative helicity and
781 bulk shear in supercell thunderstorm environments. *Wea. Forecasting*, **22**, 102–115.

782 Thompson, R. L., B. T. Smith, J. S. Grams, A. R. Dean, and C. Broyles, 2012: Convective
783 modes for significant severe thunderstorms in the contiguous United States. Part II:
784 Supercell and QLCS tornado environments. *Wea. Forecasting*, **27**, 1136–1154.
785 Weisman, M. L., and J. B. Klemp, 1984: The structure and classification of numerically
786 simulated convective storms in directionally veering wind shears. *Mon. Wea. Rev.,* **112**,
787 2479-2498.
788 Weisman, M. L, and R. Rotunno, 2000: The use of vertical wind shear versus helicity in
789 interpreting supercell dynamics. *J. Atmos. Sci*., **57**, 1452–1472.

790